Journal of Structural Geology 31 (2009) 950–959

Contents lists available at ScienceDirect

Journal of Structural Geology

journal homepage: www.elsevier.com/locate/jsg

The importance of the effective intermediate principal stress (σ'_2) to fault slip patterns

Alan P. Morris*, David A. Ferrill

Department of Earth, Material, and Planetary Sciences, Southwest Research Institute®, 6220 Culebra Road, San Antonio, TX 78238, USA

ARTICLE INFO

Article history:
Received 15 May 2007
Received in revised form 14 March 2008
Accepted 23 March 2008
Available online 13 April 2008

Keywords:
Faults
Stress analysis
Slip tendency
Rock strength
Transmissivity

ABSTRACT

In normal faulting regimes, the magnitudes and orientations of the maximum and minimum principal compressive stresses may be known with some confidence. However, the magnitude of the intermediate principal compressive stress is generally much more difficult to constrain and is often not considered to be an important factor. In this paper, we show that the slip characteristics of faults and fractures with complex or nonoptimal geometry are highly sensitive to variation or uncertainty in the ambient effective intermediate principal stress (σ'_2). Optimally oriented faults and fractures may be less sensitive to such variations or uncertainties. Slip tendency (T_s) analysis provides a basis for quantifying the effects of uncertainty in the magnitudes and orientations of all principal stresses and in any stress regime, thereby focusing efforts on the most important components of the system. We also show, for a normal faulting stress regime, that the proportion of potential surfaces experiencing high slip tendency (e.g., $T_s \geq 0.6$) decreases from a maximum of about 38% where $\sigma'_2 = \sigma'_3$, to a minimum of approximately 14% where σ'_2 is halfway between σ'_3 and σ'_1, and increases to another high of approximately 29% where $\sigma'_2 = \sigma'_1$. This analysis illustrates the influence of the magnitude of σ'_2 on rock mass strength, an observation previously documented by experimental rock deformation studies. Because of the link between fault and fracture slip characteristics and transmissivity in critically stressed rock, this analysis can provide new insights into stress-controlled fault transmissivity.

1. Introduction

Slip tendency analysis provides useful insights into the distribution of past slip on faults and fractures and the ability to predict current and future behavior of these structures (Morris et al., 1996; Lisle and Srivastava, 2004; Streit and Hillis, 2004; Collettini and Trippetta, 2007). Analysis of slip tendency (Morris et al., 1996) is predicated on:

1. The ability to calculate the state of normal and shear stress for a fault or fracture of any orientation within a stress tensor (e.g., Ramsay, 1967).
2. The assumption that the resolved shear and normal stresses on a surface are strong predictors of both the likelihood and direction of slip on that surface (Wallace, 1951; Bott, 1959; Lisle and Srivastava, 2004).

Although valid at all levels of stress within the Earth's crust, the analysis is most likely to yield useful information about potential slip in situations where the rock mass is critically stressed (e.g., Stock et al., 1985) and therefore contains numerous fault and fracture surfaces that may experience slip. In this paper we apply slip tendency analysis to investigate the role of the intermediate principal stress, σ_2, in determining patterns of slip tendency and potential slip directions.

Faults provide important pathways for subsurface fluid flow in many geologic settings (e.g., Sibson, 2000) including aquifers, geothermal reservoirs, and hydrocarbon reservoirs. Faults act as both conduits for and barriers to flow and are therefore the primary structural determinants of aquifer and reservoir compartmentalization and major factors in determining transmissivity anisotropy (e.g., Ferrill et al., 1999, 2000). Fault transmissivity behavior in many hydrocarbon reservoirs is dynamic on the time scale of years during the changing stress conditions generated by hydrocarbon production. Slip tendency analysis (Morris et al., 1996) has been used successfully to characterize fault slip likelihood (e.g. Ferrill et al., 1998; Streit and Hillis, 2004) and fault slip directions (Lisle and Srivastava, 2004; Collettini and Trippetta, 2007) in stress regimes associated with normal, reverse, and strike-slip faulting. Under anisotropic stress conditions, fractures in high slip tendency orientations are, in many cases, better flow conduits than fractures in low slip tendency orientations (Barton

* Corresponding author.
E-mail address: amorris@swri.org (A.P. Morris).

0191-8141/$ – see front matter © 2008 Elsevier Ltd. All rights reserved.
doi:10.1016/j.jsg.2008.03.013

et al., 1995; Morris et al., 1996; Ferrill et al., 1999; Sibson, 2000). The effect of stress anisotropy is greatest when the effective stress conditions on a fault or fracture approach those required for slip—the so-called critical stress (Stock et al., 1985; Townend and Zoback, 2000; Wiprut and Zoback, 2002; Zhang et al., 2007). Thus, preferential fluid flow through fault and fracture pathways is more pronounced the greater the differential stress (the difference between maximum and minimum principal stresses) and the greater the area of faults and fractures that are experiencing high slip tendency (Zoback et al., 1996; Morris et al., 1996; Ferrill et al., 1999; Takatoshi and Kazuo, 2003; Rogers, 2003; Chanchani et al., 2003; Sanderson and Zhang, 2004). In addition to the increased transmissivity of faults and fractures experiencing high slip tendency, experimental and field evidence suggest that even small shear displacements can impart flow anisotropy to a fault or fracture such that transmissivity is greatest perpendicular to the slip vector and within the fracture plane (Esaki et al., 1999; Ferrill and Morris, 2003; Koyama et al., 2004; Auradou et al., 2006). This effect can be strongly enhanced where faults cut and refract through a mechanically layered sequence (Ferrill and Morris, 2003). Thus, both slip tendency and potential slip direction are of interest in reservoir characterization. We show that the intermediate principal stress, σ_2, exerts a strong influence on the slip characteristics of faults with complex or nonoptimal geometry, and therefore has potential to influence the transmissivity of fault and fracture systems. Although our analysis is focused on normal fault systems, the principles also apply to other faulting regimes (Fig. 1). Slip tendency analysis provides at least a partial explanation for experimental observation that intermediate principal stress magnitude strongly influences rock strength (e.g., Handin et al., 1967).

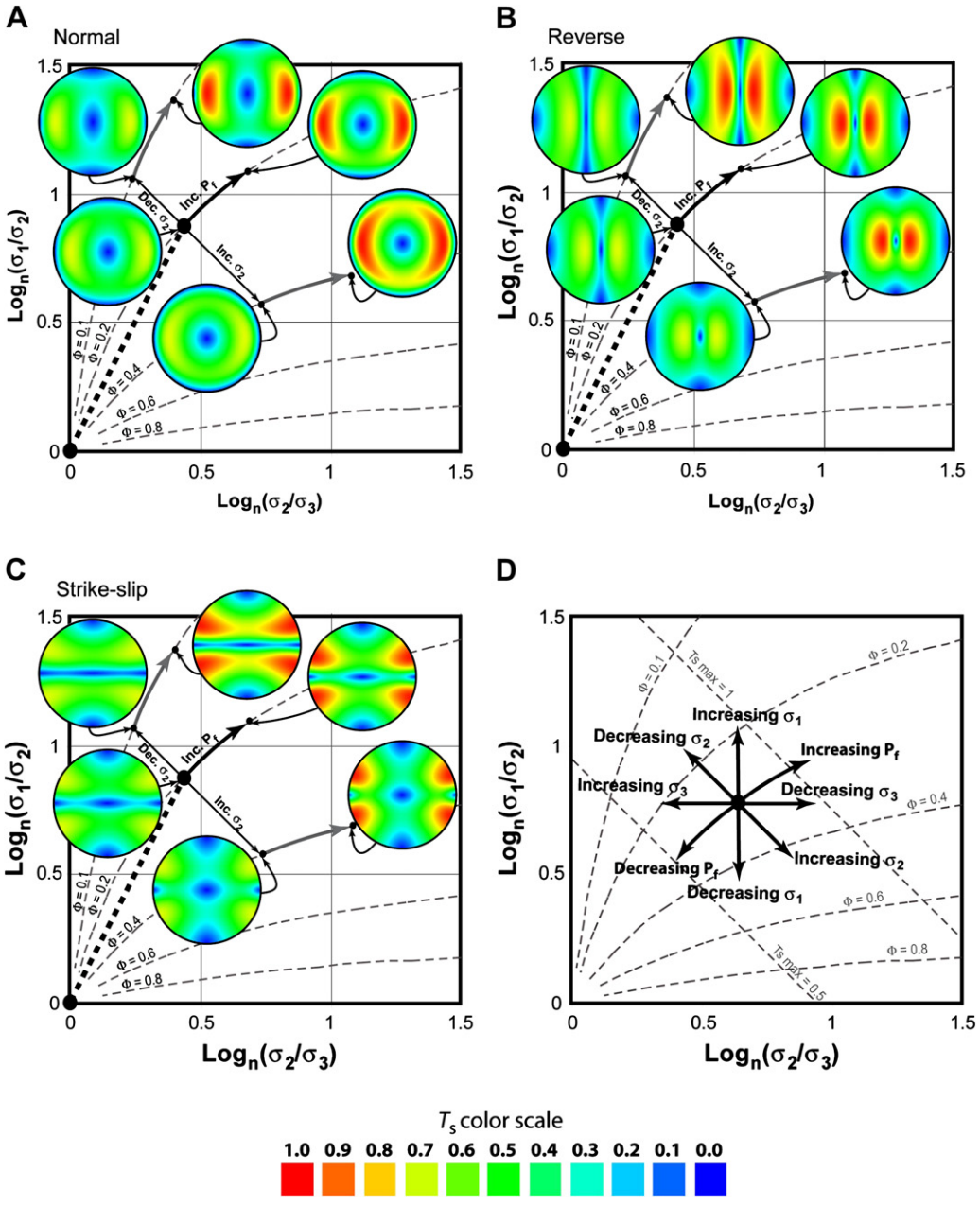

Fig. 1. Stress ratio graphs for (A) normal (σ'_1 = vertical, σ'_2 = horizontal NS, σ'_3 = horizontal EW), (B) reverse (σ'_1 = horizontal EW, σ'_2 = horizontal NS, σ'_3 = vertical), and (C) strike-slip (σ'_1 = horizontal NS, σ'_2 = vertical, σ'_3 = horizontal EW) faulting regimes. Insets are slip tendency plots (lower hemisphere plots of poles to planes of all possible orientations color-coded by slip tendency for the stress state indicated). (D) Stress ratio graph illustrating the effect of changing components of the stress tensor. See text for details. $\Phi = (\sigma'_2 - \sigma'_3)/(\sigma'_1 - \sigma'_3)$, $T_s = \tau/\sigma'$.

2. Stress measurements in hydrocarbon reservoirs

A wide spectrum of techniques has been used to determine stress conditions within the Earth's crust, including those extant in oil field and aquifer settings (Table 1). In normal faulting regimes, the maximum principal compressive stress (σ_1) is vertical (σ_v). In this case, the intermediate (σ_2) and least (σ_3) principal compressive stresses are horizontal, and often referred to as the maximum (σ_H) and minimum (σ_h) horizontal stresses, respectively. Structural geologists commonly adhere to the convention that compressive stresses are positive; in this paper, we assume that "compressive" is implicit, and we refer simply to principal stresses. The term "effective" with reference to stress signifies that the stress value has been corrected by subtracting the pore fluid pressure (Pf) in the rock (e.g., Secor, 1965). In hydrocarbon reservoirs, the vertical (lithostatic) stress is typically known with uncertainties of 5–10% from density logs acquired during drilling, and the least horizontal stress can be measured with similar precision using leak-off tests and borehole breakout information (Bolås and Hermanrud, 2002; Valley and Evans, 2007). However, measurement of the maximum horizontal stress, which in normal faulting regimes is the intermediate principal stress (σ_2), is considerably more difficult and has greater uncertainty (Bolås and Hermanrud, 2002).

In the ideal case, we would want full knowledge of the three principal stresses, fluid pressures, and the friction and cohesion characteristics of the rocks under consideration. This ideal data suite is generally not available, however, and analyses must often be performed using incomplete data. The important effect of σ_2 on potential slip characteristics and hence permeability, combined with the difficulty of obtaining precise σ_2 measurements, requires a new approach that uses available data. The influence of σ_2 can vary both from site to site and dynamically, for example during hydrocarbon production; therefore, this approach explores the range of possible stress scenarios and their implications within the bounds placed by the available data.

3. Effect of σ'_2 on slip tendency and slip direction in normal faulting regimes

3.1. Theoretical background

Slip tendency (T_s) is the ratio of maximum resolved shear stress to normal stress acting on a surface and is therefore sensitive to the orientation of the surface of interest and the form of the stress tensor (Morris et al., 1996).

$$T_s = \frac{\tau}{\sigma'_n} \tag{1}$$

where T_s is the slip tendency, τ is the maximum resolved shear stress on the surface of interest, and σ'_n is the effective normal stress on the surface of interest.

In this paper, we consider the effective stresses acting on the surface(s) of interest, which implicitly accounts for the effects of pore fluid pressure (Terzaghi, 1936). Slip tendency is a measure of the relative likelihood that a fault or fracture will undergo slip. Slip will occur if the resolved shear stress overcomes the shear strength of the fault, fracture, or rock, and the frictional resistance to sliding. Whether or not slip actually occurs will depend on the details of local conditions such as rock or fault cohesive strength, the coefficient of internal friction, and the orientation of the fault or fracture surface. In terms of the effective principal stresses, which incorporates the influence of pore fluid pressure, slip tendency (T_s) of a surface is defined as follows:

$$T_s = \frac{\sqrt{(\sigma'_1-\sigma'_2)^2 l^2 m^2 + (\sigma'_2-\sigma'_3)^2 m^2 n^2 + (\sigma'_3-\sigma'_1)^2 n^2 l^2}}{\sigma'_1 l^2 + \sigma'_2 m^2 + \sigma'_3 n^2} \tag{2}$$

where σ'_1 is the effective maximum principal stress, σ'_2 is the effective intermediate principal stress, σ'_3 is the effective minimum principal stress, l is the direction cosine of the pole to the plane with respect to σ'_1, m is the direction cosine of the pole to the plane with respect to σ'_2, and n is the direction cosine of the pole to the plane with respect to σ'_3 (Ramsay, 1967; Morris et al., 1996).

One measure of the shape of the stress tensor that is especially useful in the context of this analysis is the stress ratio Φ, where $\Phi = (\sigma'_2 - \sigma'_3)/(\sigma'_1 - \sigma'_3)$ (Lisle et al., 2006). Φ is complementary to the stress difference ratio R, where $R = (\sigma'_1 - \sigma'_2)/(\sigma'_1 - \sigma'_3)$ as used by Morris et al. (1996). Fig. 1 illustrates how patterns and values of slip tendency can vary with the shape of the stress tensor. Graphs of tensor shape in the form $\log_n(\sigma'_1/\sigma'_2)$ versus $\log_n(\sigma'_2/\sigma'_3)$ permit stress tensors to be plotted as single points (Morris et al., 1996). Three such plots are shown (Fig. 1A–C) one each for normal, reverse, and strike-slip stress regimes. Lines of equal Φ are drawn on the plots as fine dashed lines. Fig. 1A illustrates the evolution of a hypothetical sedimentary rock mass that experiences burial in a normal faulting stress regime. As burial proceeds the rock mass will experience a transition from a hydrostatic stress state where the three principal stress are equal (the origin of this graph) to the ambient normal stress regime as burial and lithification continue. This transition is represented diagrammatically by the heavy black dashed line, but may have a different and complex form. Once

Table 1
Methods of stress measurement and the information they can provide

Method	Magnitudes								Orientations					References
	σ1	σ2	σ3	σV	σH	σh	Pf	σd	σ1	σ2	σ3	σH	σh	
Focal Mechanism Stress Inversion	e	e	e											Gephart and Forsyth, 1984
Fault Population Analysis	e	e	e											Angelier, 1984; Lisle et al., 2006 and references therein
Calcite Twin Sets								p						Jamison and Spang, 1976
Calcite Twin Stress Inversion									p	p	p			Laurent et al., 1981, 1990; Lacombe and Laurent, 1992
Overburden Stress Estimation (ρgh)														Engelder, 1993
Leak-Off Testing														
Mud Weight Inversion/Fracture Pressure Gradient														Engelder, 1993
Hydraulic Fracture Analysis			e											Engelder, 1993 and references therein
Friction Curves														Engelder, 1993
Borehole Breakouts and Drilling-Induced Fractures														Engelder, 1993 and references therein
Time-Dependent or Anelastic Strain Recovery														Engelder, 1993 and references therein
Poisson's Ratio Extrapolation														Engelder, 1993

e = *Effective stress*
p = *Calcite deformation twins reflect crystal-plastic deformation, probably represent prefailure (prefaulting) stress conditions (e.g., Ferrill and Groshong, 1993; Ferrill, 1998)* σ_d = *Differential stress*

lithified the rock may experience increased pore pressure by, for example, becoming charged with hydrocarbons or becoming overpressured as some sedimentary layers are unable to dewater during compaction. Increasing pore pressure (P_f) will drive the stress tensor along a line of equal Φ (heavy black arrow in Fig. 1A). Changes in the intermediate principal stress, σ'_2, will drive the stress tensor to higher (increasing σ'_2) or lower (decreasing σ'_2) Φ values parallel to the fine solid black arrows (Fig. 1A). Lower hemisphere, equal angle projections of poles to all possible orientations, color-coded by slip tendency experienced by the surface for each pole, are given for six possible stress states. Changes in the ratio Φ are caused by changes in the relative values of the principal stresses and this causes changes in the pattern and magnitude of slip tendency distribution (Fig. 1A–D). Variation in pore pressure alone will not affect Φ and will therefore change only the magnitudes of slip tendency but not patterns of slip tendency distribution (Fig. 1D).

In the normal faulting regime, given a set of σ'_1 (vertical) and σ'_3 values for any arbitrary plane, the relationship between slip tendency (T_s) and the intermediate principal stress (σ'_2) is nonlinear, as illustrated in Fig. 2A,B. For example, in the limiting case where σ'_2 is equal to σ'_3 ($\Phi = 0$), three faults with different strikes but the same 60° dips (labeled Optimal Fault, Nonoptimal Fault 1, and Nonoptimal Fault 2 in Fig. 2A,B) will experience approximately the maximum slip tendency that can be developed in the stress state (Fig. 2A). As σ'_2 increases to the limit where σ'_2 is equal to σ'_1 ($\Phi = 1$), slip tendency on Nonoptimal Fault 2 decreases nonlinearly to zero. Slip tendency on Nonoptimal Fault 1 decreases to a minimum at about $\sigma'_2 = 80$ MPa ($\Phi = 0.79$) and increases slightly toward the limit. The Optimal Fault experiences no change

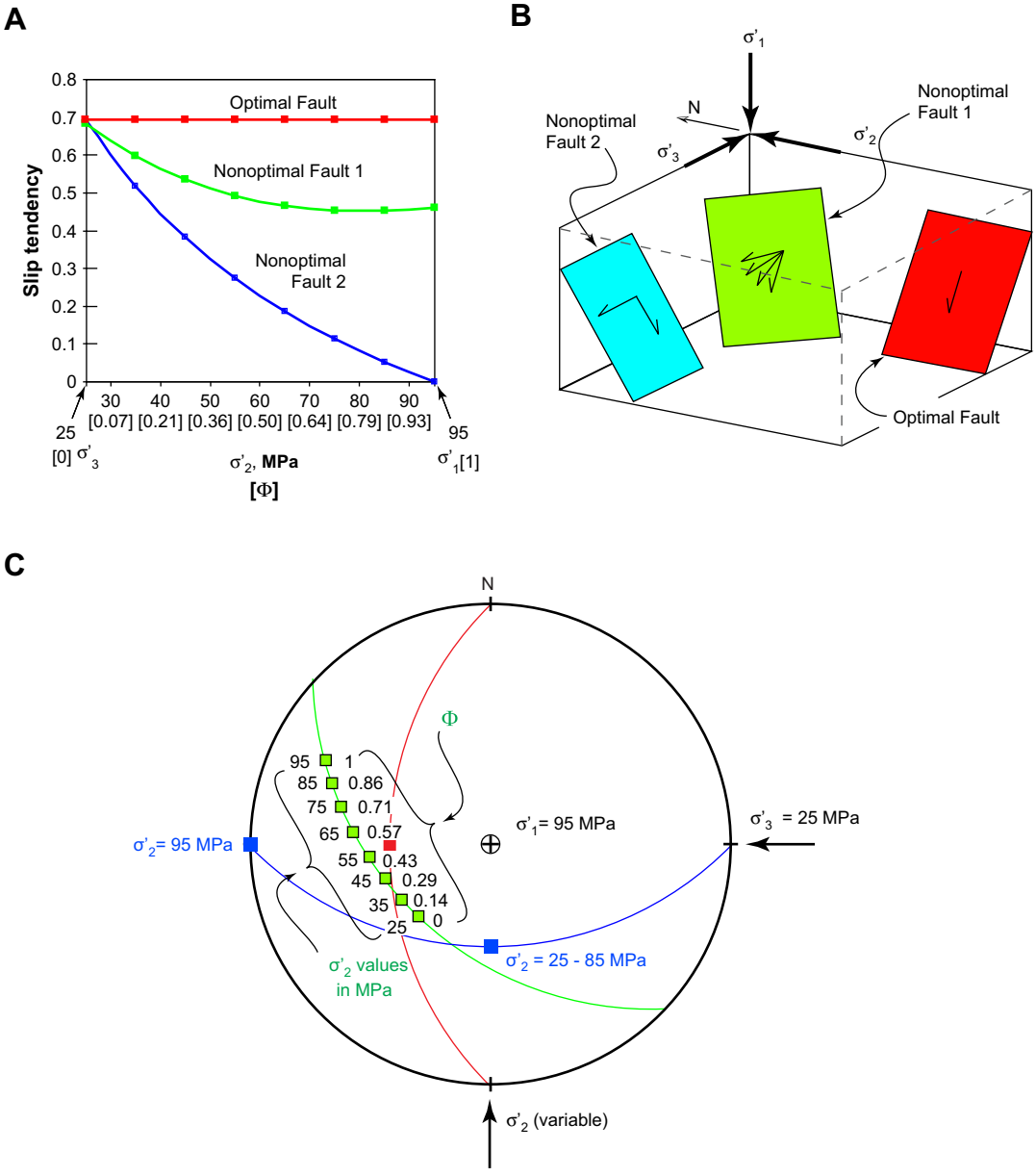

Fig. 2. (A) Plot of slip tendency versus σ'_2 for three fault orientations. The orientations of the principal stresses are constant, as are the values of σ'_1 and σ'_3. σ'_2 varies between the values of σ'_3 and σ'_1. For the optimally oriented fault (red), the value of slip tendency is invariant; however, for nonoptimally oriented faults, slip tendency varies nonlinearly with σ'_2. (B) Oblique view of the three faults schematically illustrating the variation in slip vector (maximum resolved shear stress) with variation in σ'_2. (C) Lower hemisphere projection of slip vectors for the three faults illustrated in (B). Slip direction (red square) on the Optimal Fault (red great circle) is dip slip and insensitive to variation in σ'_2. Slip direction (green squares) on Nonoptimal Fault 1 (green great circle) is sensitive to variation in σ'_2. The slip direction (blue squares) on Nonoptimal Fault 2 (blue great circle) is dip slip except when $\sigma'_2 = \sigma'_1$, in which case the slip vector is strike slip.

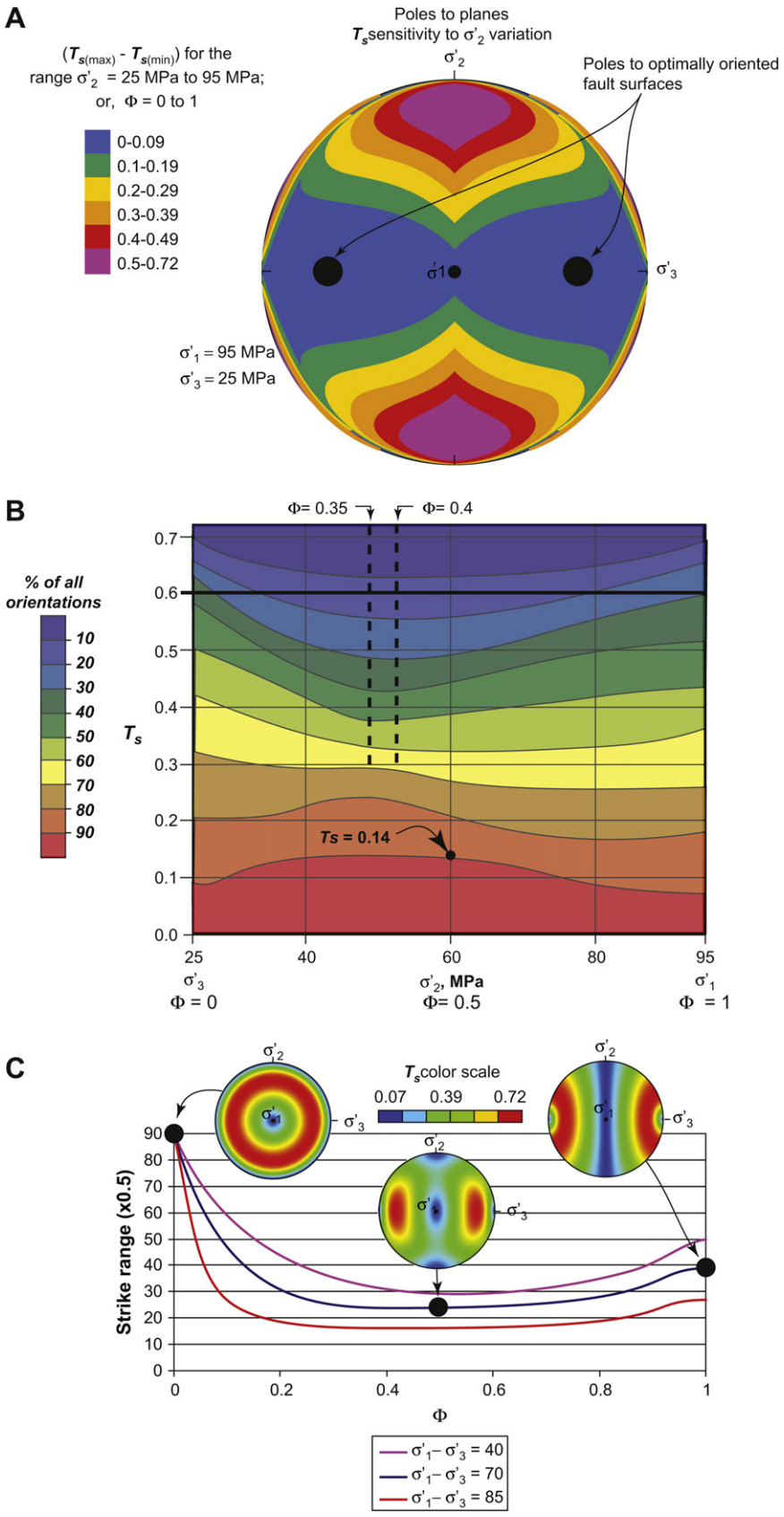

Fig. 3. Sensitivity of slip tendency to variation in σ'_2, defined as $(T_{s(max)} - T_{s(min)})$ for a range of σ'_2 values, in a normal faulting stress regime. σ'_1 is vertical and equal to 95 MPa, and σ'_3 is horizontal, east–west directed, and equal to 25 MPa. (A) Lower hemisphere plot of poles to planes of all orientations, color-coded by range of slip tendency in the range $\sigma'_3 \leq \sigma'_2 \leq \sigma'_1$. Sensitivity to σ'_2 is greatest for planes that are nonoptimally oriented. (B) Sensitivity of slip tendency viewed as percentage of all possible orientations experiencing a given slip tendency or greater as a function of varying σ'_2 for the same stress state as in (A). (C) Range of fault strikes for which appropriately dipping faults will experience 90% of the maximum slip tendency plotted versus Φ, for three values of differential stress $(\sigma'_1 - \sigma'_3)$ in a normal faulting stress regime. Insets are slip tendency plots for $\Phi = 0$, 0.5, and 1 for $(\sigma'_1 - \sigma'_3) = 70$ MPa. See text for further explanation.

in slip tendency (Fig. 2A). In addition to the variation in slip tendency, the two nonoptimal faults also experience variations in slip direction (Fig. 2B,C). Defining the variability of slip tendency as the range (maximum minus minimum) for any given planar surface as σ'_2 varies between fixed σ'_3 and σ'_1 values (Φ varies from 0 to 1), it is possible to plot this variability in slip tendency for all possible orientations. Fig. 3A is a lower hemisphere projection of poles to all possible planar surface orientations. Each pole is color-coded by the magnitude of slip tendency variation experienced by the surface it defines as σ'_2 varies between fixed σ'_3 and σ'_1 values. Variability in slip tendency is low for fault surfaces with orientations close to those of the optimum (in this case with near N–S strike and 60° dip), but increases to as much as 0.7 for faults with highly nonoptimal orientations. In other words, the magnitude of σ'_2 strongly influences the slip tendency developed on surfaces that have nonoptimal orientations for slip. A plot such as Fig. 3A would appear similar for similar values of Φ (depending on orientations of the principal stresses) but the absolute values of slip tendency variability will depend on the magnitude of the differential stress ($\sigma'_1 - \sigma'_3$). The propensity for variations in σ'_2 to change slip tendency on any surface can be summarized by plotting slip tendency against σ'_2 relative to σ'_1 and σ'_3, or Φ, and contouring points for the percentage of all orientations experiencing that slip tendency or greater, at that value of σ'_2 (Fig. 3B). In the example considered in Fig. 3B when σ'_2 has a value of 60 MPa ($\Phi = 0.5$), 90% of all surfaces will experience slip tendencies greater than 0.14.

3.2. Effect of σ'_2 on fault strike direction

In the normal faulting regime, it is common to assume that faults develop in conjugate sets, forming a bimodal fault population with oppositely dipping maxima. The line of intersection between faults of the two sub-populations is the intermediate principal stress (σ'_2) direction (Anderson, 1951). This is essentially the case where σ'_2 is mid-way between σ'_3 and σ'_1, i.e. $\Phi = 0.5$ (Fig. 3C). In nature, however, there is no strict constraint on the value of σ'_2 with respect to σ'_3 and σ'_1, and all conditions can exist from $\sigma'_2 = \sigma'_3$ ($\Phi = 0$; e.g., caldera collapse, deformation above a dome, and polygonal faulting; Cartwright et al., 2003) to $\sigma'_2 = \sigma'_1$ ($\Phi = 1$; e.g., close coexistence of normal and strike-slip faults, Stock et al., 1985; Morris et al., 1996). A corollary of this is that fault strike directions are not tightly constrained except where Φ is close to 0.5 (Fig. 3C).

3.3. Effect of σ'_2 on rock strength

This analysis of slip tendencies developed on all possible orientations can provide some insight into the influence of the intermediate principal stress on the strength of rock. Consider, for example, the percentage of all orientations that experience a slip tendency of 0.6 or greater. When $\sigma'_2 = \sigma'_3$, 35% of orientations equal or exceed $T_s = 0.6$. With increasing Φ, the percentage of surfaces with $T_s \geq 0.6$ drops to a minimum of 14% at $\Phi = 0.5$, and rises to another maximum at $\Phi = 1$ where 29% of orientations experience $T_s \geq 0.6$. Variation as a function of Φ exists for all values of slip tendency (Fig. 3B). This variation implies that if, for example, a slip tendency of 0.6 (heavy black horizontal line) were the threshold for slip in the situation under consideration, there would be 6% fewer opportunities for slip to occur when $\sigma'_2 = \sigma'_1$ than when $\sigma'_2 = \sigma'_3$, and 21% fewer opportunities for slip when σ'_2 is approximately mid-way between σ'_3 and σ'_1. Thus there is a general inherent geometric strengthening of rock as σ'_2 increases. Potential rock strength, viewed in this way, exhibits a "strong spot" at about $\Phi = 0.35$–0.4 (vertical dashed lines in Fig. 3B). Our analysis indicates that traditional triaxial testing of rocks (where $\sigma'_2 = \sigma'_3$) takes place under conditions that maximize the number of surfaces experiencing high slip tendencies (say, above 0.3) and therefore represents the weakest stress conditions for a rock. This helps explain the experimental observation that under true triaxial stress conditions ($\sigma'_1 > \sigma'_2 > \sigma'_3$) rock strength increases non-linearly with the magnitude of σ'_2 for fixed σ'_1 and σ'_3 (e.g., Handin et al., 1967; Haimson, 2003, and references therein).

3.4. Analysis of individual real fault geometries

At the scale of mappable or imageable faults, individual faults can be considered to consist of a population of contiguous, quasi-planar patches with a range of orientations (Fig. 4A,B). In the example presented here, two faults (labeled 002 and 009) from offshore Canada and interpreted from proprietary three-dimensional reflection seismic data are used to illustrate this analysis. Each fault can be analyzed for its sensitivity to changes in magnitude of σ'_2. The faults are "illuminated" by a stress field in which σ'_1 is vertical and varies with depth according to an assumed sediment density profile (Fig. 4C), and σ'_3 is oriented E–W and for simplicity is assumed to be 0.3 of σ'_1. The intermediate effective principal stress, σ'_2, is oriented N–S, and its magnitude is varied from that of σ'_3 to that of σ'_1. For predictive analysis, uncertainty in the knowledge of some measure, in this case the magnitude of σ'_2, can be modeled as variation in that value. In the following analysis, variation and uncertainty are associated in this sense but are not considered synonymous. For each increment of σ'_2, interpreted fault surfaces are analyzed for slip tendency variation and the area across which that slip tendency is active. Fig. 5A–C illustrate the three-dimensional appearance of this analysis for three conditions of σ'_2. Synopses of all these variations for faults 002 and 009 are shown in Fig. 6A,B, respectively. Most of the surface of fault 009 is near-optimally oriented for slip in the modeled stress state (Fig. 4A,B) and is relatively insensitive to variation or uncertainty in the magnitude of σ'_2 (Fig. 5A–C). Most of the surface of fault 002, however, is not optimally oriented for slip (Fig. 4A,B) and is much more sensitive to variation in σ'_2. Although the pattern of sensitivity of fault 002 can be seen in displays such as Fig. 5A–C, it is not easily quantifiable. Fig. 6A,B is constructed by determining the area of the fault experiencing a given slip tendency as a percentage of total fault area, then expressing this as the cumulative percentage of fault area experiencing a given slip tendency or higher. Thus, under conditions where $\Phi = 0.14$ ($\sigma'_2 = (0.4 \times \sigma'_1)$, Fig. 6A), more than 80% of fault 002 experiences slip tendencies greater than 0.4, whereas this value is 20% where $\Phi \geq 0.43$ ($\sigma'_2 \geq (0.6 \times \sigma'_1)$; Fig. 6A). Conversely, Fig. 6B illustrates the relative insensitivity of fault 009 to variation or uncertainty in the magnitude of σ'_2. As discussed above, variation in σ'_2 also causes potential slip directions to vary on non-optimally oriented fault surfaces. Variation in potential slip direction with σ'_2 magnitude can be illustrated by ordering slip directions according to their respective slip tendencies and plotting them on a stereographic projection (Fig. 6C–H). From inspection, both faults 002 and 009 experience greater variability in slip directions with increasing value of stress ratio Φ (compare Fig. 6C, D, and E and Fig. 6F, G, and H). However, comparing the angular standard deviations as one measure of the degree of variability in orientation, the near-optimally oriented fault 009 exhibits much lower sensitivity to σ'_2 values than fault 002. If fault 002 is thought to contribute significantly to compartmentalization of the reservoir or if it is considered to be a flow conduit, then variation or uncertainty in σ'_2 could warrant acquiring additional data to better constrain its value.

4. Discussion

A recent compilation and analysis of over 2000 stress tensors from shallow crustal levels from normal, strike-slip, and thrust faulting regimes shows a complete spectrum of the stress ratio,

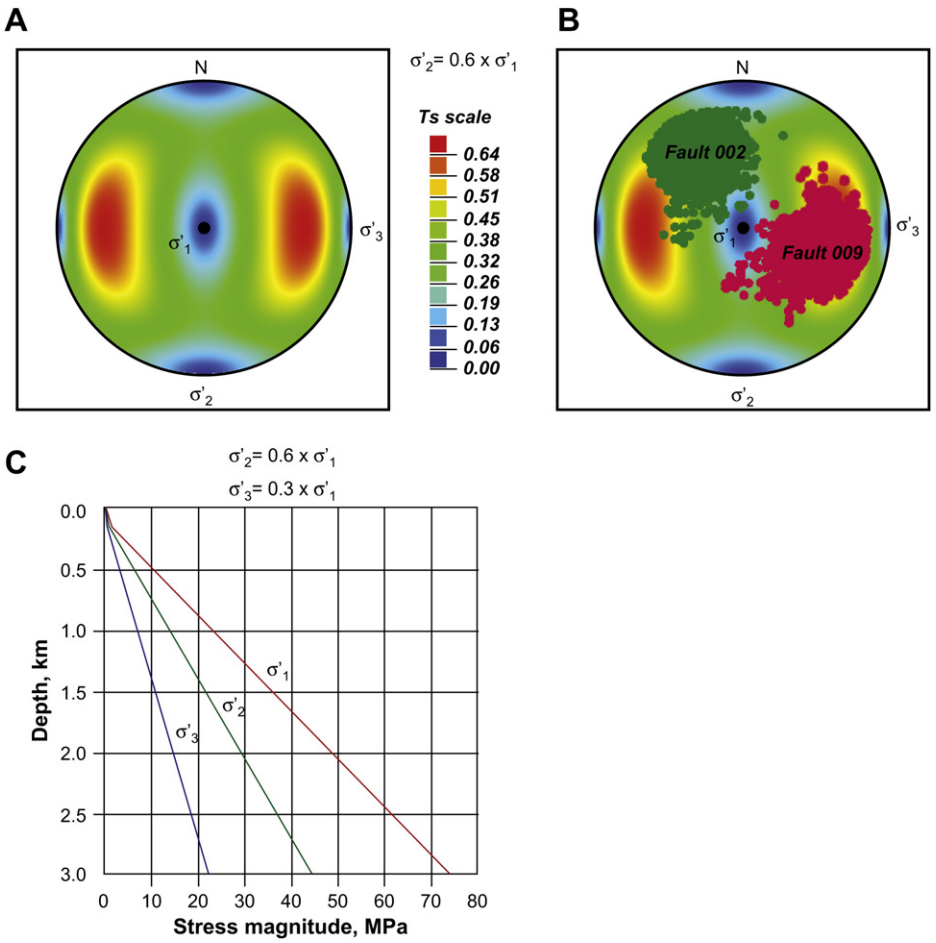

Fig. 4. (A) Slip tendency plot for the stress state: σ'_1 = vertical, σ'_3 = horizontal directed east–west, and the principal stresses vary with depth according to the graph in (C). See text for details. The slip tendency pattern under these stress conditions is invariant with depth. (B) Poles to all triangular patches of faults 002 and 009 superimposed on the slip tendency plot shown in (A). Most of fault 009 experiences moderate to high slip tendency in contrast to fault 002, which experiences moderate to low slip tendency (i.e., fault 009 is near-optimally oriented, fault 002 is nonoptimally oriented). (C) Stress versus depth plot for the stress state used to calculate plots in (A) and (B).

Φ $((\sigma'_2 - \sigma'_3)/(\sigma'_1 - \sigma'_3))$, ranging from 0 to 1 (Lisle et al., 2006). Average values are 0.34, 0.40, and 0.43 for normal, strike-slip, and thrust faulting regimes, respectively, demonstrating the widespread deviation of σ'_2 from a value midway between σ'_1 and σ'_3 ($\Phi = 0.5$). This is further documented by the occurrence of stress regimes where σ'_2 and σ'_1 are close in magnitude, resulting in short-term temporal switching between normal and strike-slip faulting (e.g., Stock et al., 1985; Bellier and Zoback, 1995; Morris et al., 1996).

It is well known that faults tend to be weak, in many cases slipping at relatively low slip tendencies rather than the highest possible slip tendencies indicated by values of internal friction (Kubo and Fukuyama, 2003; Moore, 2005; Collettini and Trippetta, 2007). The apparent "weakness" of many real faults, and variability in slip tendency necessary for slip, requires that slip tendency values be calibrated for the setting in which the analysis is being performed. Fully lithified rocks may have considerably different slip tendency behavior from relatively unlithified sediments such as those in oilfield settings in the Gulf of Mexico. Mode of slip may also be important; there is evidence to suggest that faults experiencing aseismic creep may be less likely to become "leaky" than those slipping seismically (Wilkins and Naruk, 2007). Actual slip on a fracture or fault surface may not be required for permeability effects to become important—precursor fracture formation and fracture dilation may enhance permeability prior to slip. This is also likely to be affected by rock type and deformation setting. However, the threshold(s) at which significant permeability changes occur can be estimated from both laboratory experiments and field studies (e.g. Finkbeiner et al., 1997; Lunn, 2005).

There is strong evidence to suggest that faults and fractures that experience high slip tendency within a critically stressed system are more likely to be transmissive with respect to fluids than faults and fractures experiencing low slip tendencies (Zoback et al., 1996; Morris et al., 1996; Ferrill et al., 1999; Takatoshi and Kazuo, 2003; Rogers, 2003; Chanchani et al., 2003). In addition, experimental and field evidence suggest that small shear displacements can impart directional flow anisotropy to a fault or fracture such that transmissivity is greatest perpendicular to the slip vector and within the fracture plane (Esaki et al., 1999; Ferrill and Morris, 2003; Koyama et al., 2004; Auradou et al., 2006). Thus the slip characteristics of fault and fracture populations within hydrocarbon reservoirs and aquifers can exert a strong influence on the bulk transmissivity of the system. We have demonstrated that the magnitude of the intermediate principal stress is a key determinant of slip tendency and slip direction on faults and fractures in the normal faulting regime. The principles of the analysis also apply to other stress regimes.

The approach presented here provides a means for quantifying the uncertainty inherent in understanding the effects of faults on permeability architecture. In the case where σ'_1 and σ'_3 are well constrained but σ'_2 (σ_H in the normal faulting stress regime) is not, the question of the importance of σ'_2 and its effect on permeability arises. Using the analysis presented here, a fault interpretation can

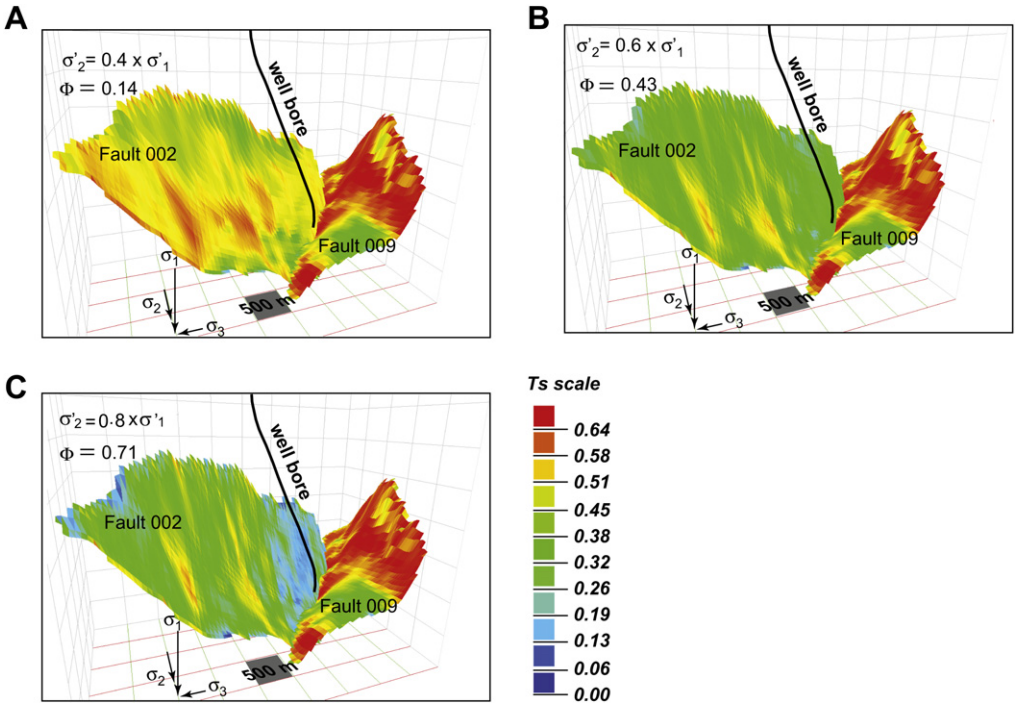

Fig. 5. (A)–(C). Oblique views of faults 002 and 009 illuminated by the stress field described in Fig. 4 and in the text. σ'_2 varies from (A) 0.4 of σ'_1 to (B) 0.6 of σ'_1 to (C) 0.8 of σ'_1. Triangular fault patches are color-coded by slip tendency.

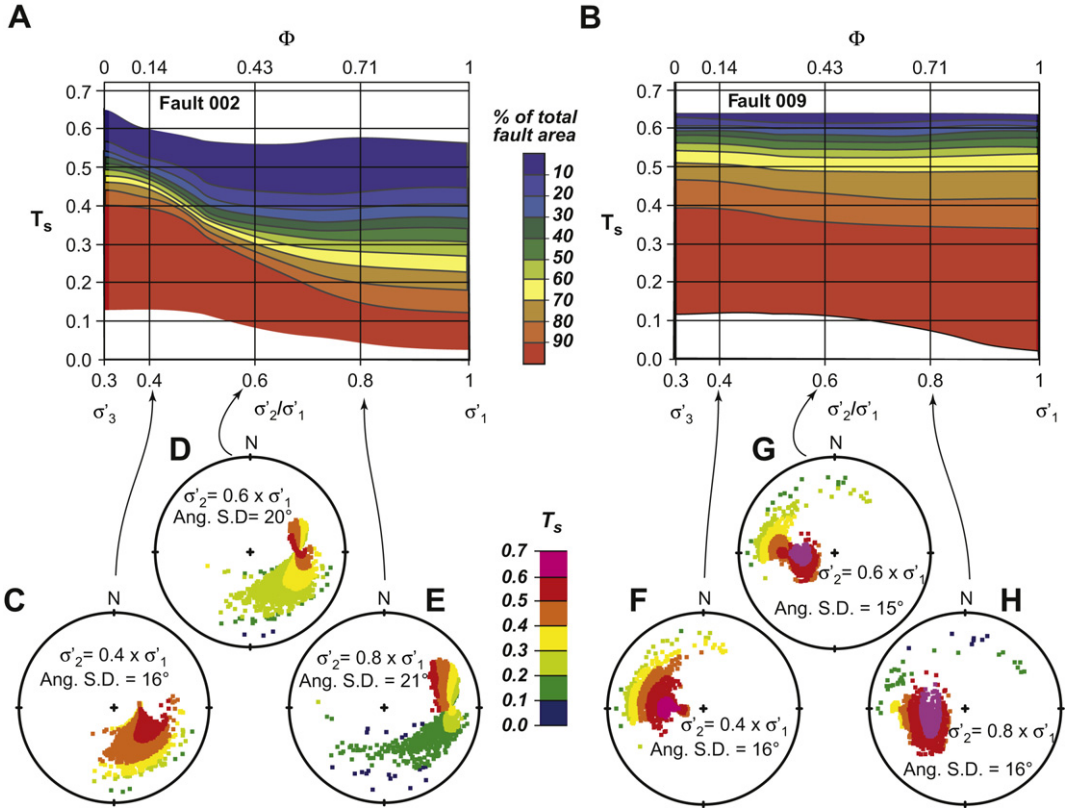

Fig. 6. (A) and (B) illustrate the sensitivity of slip tendency to variation in σ'_2 for faults 002 (A) and 009 (B). These plots are analogous to Fig. 3B, however, not all orientations are represented on each fault surface, resulting in truncated plots at both high and low slip tendency values. See text for details. (C)–(H) Lower hemisphere projections of slip vectors (direction of maximum resolved shear stress) for all triangular patches constituting faults 002 (C, D, E) and 009 (F, G, H). Vectors are colored by their slip tendency. The stress state is as described in Fig. 4 and in the text. (C) $\sigma'_2 = 0.4$ of σ'_1, angular standard deviation = 16°. (D) $\sigma'_2 = 0.6$ of σ'_1, angular standard deviation = 20°. (E) $\sigma'_2 = 0.8$ of σ'_1, angular standard deviation = 21°. (F) $\sigma'_2 = 0.4$ of σ'_1, angular standard deviation = 16°. (G) $\sigma'_2 = 0.6$ of σ'_1, angular standard deviation = 15°. (H) $\sigma'_2 = 0.8$ of σ'_1, angular standard deviation = 16°.

be analyzed for its sensitivity to variation in σ'_2 and numerical limits placed on this sensitivity. This analysis will better inform reservoir and aquifer transmissivity characterization, help evaluate the priority of resource allocation in improving estimates of σ'_2, focus data collection on key uncertainties, and inform optimization strategies as stress states change.

5. Conclusions

Ambient stress exerts a strong control on fault slip behavior, especially on faults that are not optimally oriented for slip. Although some components of the ambient stress field may be well constrained, it is common for σ'_2 to be the least understood of the three principal stresses. Variation in the magnitude of σ'_2, however, can have far-reaching effects on the slip tendency, distribution (range) of fault strike within a normal fault network, potential slip directions, and overall strength of faults and fault systems within the ambient stress state. Treating interpreted faults as contiguous assemblages of triangular patches and examining their potential behavior in varying stress fields provides data that can be used to assess the sensitivity of fault behavior to uncertainty about the value of σ'_2. This same approach can be used to analyze evolution of behavior during stress field transitions, either natural (e.g., earthquake rupture cycle) or anthropogenic (e.g., hydrocarbon production and compaction or carbon dioxide injection). This type of analysis is not limited to variation in the magnitude of σ'_2, and can be applied to other principal stress magnitudes, stress orientations (for example, stress regimes other than that of normal faulting), and time-dependent variations in stress field that occur during the production lifetime of a reservoir or aquifer. Because of the link between fault slip characteristics and fault transmissivity in critically stressed rock masses, this analysis can provide new insights into stress-controlled fault transmissivity.

Acknowledgements

We thank Nathan Franklin and Chad Zalkin for programming 3DStress®, Iain Sinclair and Judith McIntyre of Husky Energy for the use of their three-dimensional fault interpretations, and Danielle Wyrick, Lauren Mulverhill, and David Turner for helpful reviews of this manuscript. Richard Lisle and an anonymous reviewer significantly improved the final form of this paper. Conversations with Terry Engelder and Kevin Smart provided very helpful input.

References

Anderson, E.M., 1951. The Dynamics of Faulting and Dyke Formation with Applications to Britain. Oliver and Boyd, Edinburgh, UK, 206 pp.

Angelier, J., 1984. Fault slip analysis of fault slip data sets. Journal of Geophysical Research B89, 5835–5848.

Auradou, H., Drazer, G., Boschan, A., Hulin, J.-P., Koplik, J., 2006. Flow channeling in a single fracture induced by shear displacement. Geothermics 35, 576–588.

Barton, C.A., Zoback, M.D., Moos, D., 1995. Fluid flow along potentially active faults in crystalline rock. Geology 23, 683–686.

Bellier, O., Zoback, M.L., 1995. Recent state of stress change in the Walker Lane zone western Basin and Range province, United States. Tectonics 14, 564–593.

Bolås, H.M.N., Hermanrud, C., 2002. Rock stress in sedimentary basins – implications for trap integrity. In: Koestler, A.G., Hunsdale, R. (Eds.), Hydrocarbon Seal Quantification. Special Publication, vol. 11. Norwegian Petroleum Society, pp. 17–35.

Bott, M.H.P., 1959. The mechanics of oblique slip faulting. Geological Magazine 96, 109–117.

Cartwright, J., James, D., Bolton, A., 2003. The genesis of polygonal fault systems; a review. In: van Rensbergen, P., Hillis, R., Maltman, A.-J., Morley, C.-K. (Eds.), Subsurface Sediment Mobilization. Special Publications, vol. 216. Geological Society, London, pp. 223–243.

Chanchani, S.K., Zoback, M.D., Barton, C., 2003. A case study of hydrocarbon transport along active faults and production-related stress changes in the Monterey Formation, California. In: Ameen, M. (Ed.), Fracture and In-Situ Stress Characterization of Hydrocarbon Reservoirs. Special Publication, vol. 209. Geological Society, London, pp. 17–26.

Collettini, C., Trippetta, F., 2007. A slip tendency analysis to test mechanical and structural control on aftershock rupture planes. Earth and Planetary Science Letters 255, 402–413.

Engelder, T., 1993. Stress Regimes in the Lithosphere. Princeton University Press, Princeton, NJ.

Esaki, T., Du, S., Mitani, Y., Ikusada, K., Jing, L., 1999. Development of a shear-flow test apparatus and determination of coupled properties for a single rock joint. International Journal of Rock Mechanics and Mineral Science 36, 641–650.

Ferrill, D.A., 1998. Critical re-evaluation of differential stress estimates from calcite twins. Tectonophysics 285, 77–84.

Ferrill, D.A., Groshong Jr., R.H., 1993. Deformation conditions in the northern Subalpine Chain, France, estimated from deformation modes in coarse-grained limestone. Journal of Structural Geology 15, 995–1006.

Ferrill, D.A., Morris, A.P., Jones, S.M., Stamatakos, J.A., 1998. Extensional layer-parallel shear and normal faulting. Journal of Structural Geology 20, 355–362.

Ferrill, D.A., Morris, A.P., 2003. Dilational normal faults. Journal of Structural Geology 25, 183–196.

Ferrill, D.A., Winterle, J., Wittmeyer, G., Sims, D., Colton, S., Armstrong, A., Morris, A. P., 1999. Stressed rock strains groundwater at Yucca Mountain, Nevada. GSA Today 9, 1–8.

Ferrill, D.A., Morris, A.P., Stamatakos, J.A., Sims, D.W., 2000. Crossing conjugate normal faults. American Association of Petroleum Geologists Bulletin 84, 1543–1559.

Finkbeiner, T., Barton, C.A., Zoback, M.D., 1997. Relationships among in-situ stress, fractures and faults, and fluid flow: Monterey Formation, Santa Maria Basin, California. American Association of Petroleum Geologists Bulletin 81, 1975–1999.

Gephart, J.W., Forsyth, D., 1984. An improved method for determining the regional stress tensor using earthquake focal mechanism data: application to the San Fernando earthquake sequence. Journal of Geophysical Research 89, 9305–9320.

Haimson, B., 2003. Strength, deformability, and micromechanics of brittle fracture in a crystalline rock under true triaxial compressive stresses. ISRM 2003-Technology Roadmap for Rock Mechanics. South African Institute of Mining and Metallurgy, 451–456.

Handin, J., Heard, H.C., Magouirk, J.N., 1967. Effect of the intermediate principal stress on the failure of limestone, dolomite, and glass at different temperature and strain rate. Journal of Geophysical Research 72, 611–640.

Jamison, W.R., Spang, J.H., 1976. Use of calcite twin lamellae to infer differential stress. Bulletin of the Geological Society of America 87, 868–872.

Koyama, T., Fardin, N., Jing, L., 2004. Shear induced anisotropy and heterogeneity of fluid flow in a single rock fracture by translational and rotatory shear displacements – a numerical study. Paper 2A 08-SINOROCK2004 Symposium, 426.

Kubo, A., Fukuyama, E., 2003. Stress fields and fault reactivation angles of the 2000 western Tottori aftershocks and the 2001 northern Hyogo swarm in southwest Japan. Tectonophysics 378, 223–239.

Lacombe, O., Laurent, P., 1992. Determination of principal stress magnitudes using calcite twins and rock mechanics data. Tectonophysics 202, 83–97.

Laurent, P., Bernard, P., Vasseur, G., Etchecopar, A., 1981. Stress tensor determination from the study of e-twins in calcite: a linear programming method. Tectonophysics 78, 651–660.

Laurent, P., Tourneret, C., Laborde, O., 1990. Determining deviatoric stress tensors from calcite twins: applications to monophase synthetic and natural polycrystals. Tectonics 9, 379–389.

Lisle, R.J., Srivastava, D.C., 2004. Test of the frictional reactivation theory for faults and validity of fault-slip analysis. Geology 32, 569–572.

Lisle, R.J., Orife, R.O., Arlegui, L., Liesa, C., Srivastava, D.C., 2006. Favored states of palaeostress in the Earth's crust: evidence from fault-slip data. Journal of Structural Geology 28, 1051–1066.

Lunn, R.J., 2005. Investigating the relationship between fault permeability, pore pressure and effective stress using constraints from reservoir induced seismicity. Geological Society of America Abstracts with Programs 37, 167.

Moore, D., 2005. Review of evidence for a weak San Andreas Fault. Geophysical Research Abstracts 7, 05878.

Morris, A.P., Ferrill, D.A., Henderson, D.B., 1996. Slip tendency and fault reactivation. Geology 24, 275–278.

Ramsay, J.G., 1967. Folding and Fracturing of Rocks. McGraw Hill, New York.

Rogers, S.F., 2003. Critical stress-related permeability in fractured rocks. In: Ameen, M. (Ed.), Fracture and In-Situ Stress Characterization of Hydrocarbon Reservoirs. Special Publication, vol. 209. Geological Society, London, pp. 7–16.

Sanderson, D.J., Zhang, X., 2004. Stress controlled localisation of deformation and fluid flow in fractured rocks. Geological Society of London Special Publication 231, 299–314.

Secor, D.T., 1965. Role of fluid pressure in jointing. American Journal of Science 263, 633–646.

Sibson, R.H., 2000. Fluid involvement in normal faulting. Journal of Geodynamics 29, 469–499.

Streit, J.E., Hillis, R.R., 2004. Estimating fault stability and sustainable fluid pressures for underground storage of CO_2 in porous rock. Energy 29, 1445–1456.

Stock, J.M., Healy, J.H., Hickman, S.H., Zoback, M.D., 1985. Hydraulic fracturing stress measurements at Yucca Mountain, Nevada, and relationship to regional stress field. Journal of Geophysical Research 90, 8691–8706.

Takatoshi, I., Kazuo, H., 2003. Role of stress-controlled flow pathways in HDR geothermal reservoirs. Pure and Applied Geophysics 160, 1103–1124.

Terzaghi von, K., 1936. The shearing resistance of saturated soils and the angle between the planes of shear. In: First International Conference on Soil Mechanics, vol. 1. Harvard University, Cambridge, MA. 54–56.

Townend, J., Zoback, M.D., 2000. How faulting keeps the crust strong. Geology 28, 399–402.
Valley, B., Evans, K.F., 2007. Stress state at Soultz-sous-Forêts to 5 km depth from wellbore failure and hydraulic observations. Proceedings of the 32nd Workshop on Geothermal Reservoir Engineering, January 22–24. Stanford University, Stanford, CA.
Wallace, R.E., 1951. Geometry of shearing stress and relationship to faulting. Journal of Geology 59, 111–130.
Wilkins, S.J., Naruk, S.J., 2007. Quantitative analysis of slip-induced dilation with application to fault seal. American Association of Petroleum Geologists Bulletin 91, 97–113.
Wiprut, D., Zoback, M.D., 2002. Fault reactivation, leakage potential, and hydrocarbon column heights in the northern North Sea. In: Koestler, A.G., Hunsdale, R. (Eds.), Hydrocarbon Seal Quantification. Special Publication, vol. 11. Norwegian Petroleum Society, pp. 203–219.
Zhang, X., Koutsabeloulis, N., Heffer, K., 2007. Hydromechanical modeling of critically stressed and faulted reservoirs. American Association of Petroleum Geologists Bulletin 91, 31–50.
Zoback, M., Barton, C., Finkbeiner, T., Dholakia, S., 1996. Evidence for fluid flow along critically-stressed faults in crystalline and sedimentary rock. In: Jones, G., Fisher, Q., Knipe, R. (Eds.), Faulting, Faults Sealing and Fluid Flow in Hydrocarbon Reservoirs. University of Leeds, UK, pp. 47–48.